

An entangled-LED driven quantum relay over 1 km

C. Varnava,^{1,2} R. M. Stevenson,^{1,*} J. Nilsson,² J. Skiba-Szymanska,² B. Dzurňák,^{2,†}
M. Lucamarini,² R. V. Penty,² I. Farrer,³ D. A. Ritchie,³ and A. J. Shields¹

¹Toshiba Research Europe Limited, 208 Science Park, Milton Road, Cambridge CB4 0GZ, UK

²Cambridge University Engineering Department, 9 J J Thomson Avenue, Cambridge CB3 0FA, UK

³Cavendish Laboratory, University of Cambridge, J J Thomson Avenue, Cambridge CB3 0HE, UK

Quantum cryptography allows confidential information to be communicated between two parties, with secrecy guaranteed by the laws of nature alone. However, upholding guaranteed secrecy over quantum communication networks poses a further challenge, as classical receive-and-resend routing nodes can only be used conditional of trust by the communicating parties. Here, we demonstrate the operation of a quantum relay over 1 km of optical fiber, which teleports a sequence of photonic quantum bits to a receiver by utilizing entangled photons emitted by a semiconductor LED. The average relay fidelity of the link is 0.90 ± 0.03 , exceeding the classical bound of 0.75 for the set of states used, and sufficiently high to allow error correction. The fundamentally low multi-photon emission statistics and the integration potential of the source present an appealing platform for future quantum networks.

The critical importance of information security in the digital age has led to the pervasive use of cryptography. The emerging field of quantum cryptography[1, 2], offers a means to guarantee the security of digital interactions which can be proven information theoretic secure. Reported quantum key distribution systems are typically based on weak-coherent optical pulses, and have evolved rapidly. Such systems allow unique cryptographic keys to be shared between directly connected users on point-to-point[3–5] or point-to-multipoint links[6].

In contrast, the situation for networks connecting multiple parties is less developed. One solution has been to demonstrate nodal networks, based on individual quantum links connected by classical intermediary systems[7]. The result of this type of network topology is that end users are required to trust the intermediary systems, which arguably diminishes the value of the underlying quantum cryptography.

To establish fully quantum multi-partite networks, it is necessary to route quantum signals through a backbone of quantum nodes. This can be achieved by leveraging quantum entanglement to set up non-local correlations between measurements by end users. Examples of such schemes are distribution of entangled photon pairs to end users, where local measurements are performed[8], or conversely, where photons are sent by two users to be projected into a Bell state by an intermediate quantum node[9–11]. Photonic quantum repeaters[12] and relays[13] employ both of these effects to teleport entangled or single qubits respectively in a manner that can be chained to create a fully quantum network for which theoretically proven quantum security can be preserved.

Here, we report operation of a quantum relay over 1 km

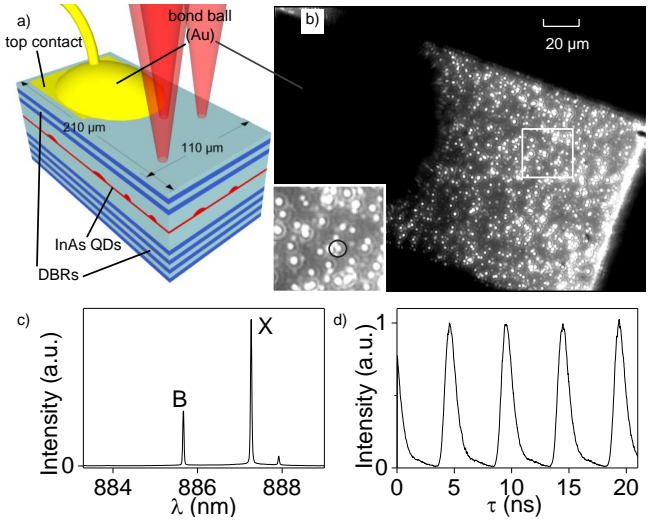


Figure 1: (a) Schematic of the ELED used in this experiment (not to scale). The entangled photon source is an InAs quantum dot (QD) embedded in a p-i-n diode structure with a cavity centred at ~ 886 nm, between top and bottom distributed Bragg reflectors (DBRs). (b) Microscope image of the mesa used for this experiment. Individual quantum dots can be identified as points of light in the image. The dark circular area is the gold bond to the top contact. The quantum dot chosen for the experiment is identified in the inset. (c) Biexciton (B) and exciton (X) electroluminescence spectrum under experimental biasing conditions. (d) Time-resolved biexciton electroluminescence.

of optical fiber using entangled photons generated by a light emitting diode to teleport photonic qubits encoded on weak coherent pulses emitted by a laser. Compared to previously reported quantum relays[14] and photonic teleportation over significant distances[15, 16], our system is directly electrically driven using a simple semiconductor device, offering a route to large-scale network deployments. Teleporting weak coherent states offers po-

*Electronic address: mark.stevenson@crl.toshiba.co.uk

†Current Address: Department of Physics and Astronomy, University of Sheffield, Sheffield S3 7RH, UK

tential enhancements to state-of-the art quantum key distribution systems, as it creates output photons with sub-Poissonian statistics immune to the photon number splitting attack[17, 18], and protects against intrusions[19].

At the heart of our quantum relay is an entangled-light-emitting diode (ELED)[20], as shown in Fig. 1(a). It consists of a layer of self-assembled indium arsenide quantum dots within a gallium arsenide microcavity (Appendix). We have optimized the resistance and capacitance of the device to allow it to be driven by short electrical pulses, without compromising entanglement fidelity or photon coherence. This has allowed electrically triggered quantum teleportation using an LED, which has previously been limited to only d.c. operation[18, 21].

An image of the ELED in operation is shown in Fig. 1(b). Individual points of light are observed, corresponding to light emission from individual quantum dots. We select emission from a chosen quantum dot, indicated in the inset image, by collection with a single mode fibre. The emission spectrum measured by a grating spectrometer and CCD camera is shown in Fig. 1(c). Two strong emission lines are observed corresponding to the first, biexciton photon (*B*) and second, exciton photon (*X*) emission. The *B* and *X* emission lines are then spectrally filtered with a diffraction grating to isolate them from each other and other emission from the device, including that originating from the quantum well-like wetting layer, and any other nearby quantum dots (such as the weak peak seen at ~ 888 nm).

The ELED was driven at a repetition rate of 203 MHz, with pulses of nominally 0.4V amplitude and 490 ps duration. Time-resolved electroluminescence was measured under these conditions and shown in Fig. 1(d) for *B* as a black line. The emission is strongly pulsed, and well contained within each cycle.

The experimental quantum relay system is shown in Fig. 2(a). It comprises 4 sections separated by three 350 m fiber optic links. The first, ‘Sender’ section is thus separated from the last ‘Receiver’ section by 1.05 km of optical fiber. Entangled photons emitted by the ELED are divided, the *B* photons are sent to the Bell-State Measurement (BSM) section, and the *X* photons are sent to the ‘Receiver’. The ‘Sender’ employs a wavelength tunable c.w. laser diode, from which pulses are generated by an external optical intensity modulator, tuned to the frequency of the ELED. The polarized pulses are then rotated by a polarization controller PC1 to encode the qubit, before transmission to the ‘BSM’ section.

At the ‘BSM’ section, an imbalanced beamsplitter BS combines 95% of the *B* photons with 5% of the laser photons into one output arm, before a polarization controller PC2 and polarizing beamsplitter projects horizontal (*H*) and vertical (*V*) polarized photons onto superconducting single photon detectors (SSPD) D1 and D2. The function of this section is to perform a Bell state measurement in the state $(|H_LV_B\rangle + |V_LH_B\rangle)/\sqrt{2}$ where subscripts *L* and *B* denote photons originating from the laser and biexciton respectively. Such a measurement col-

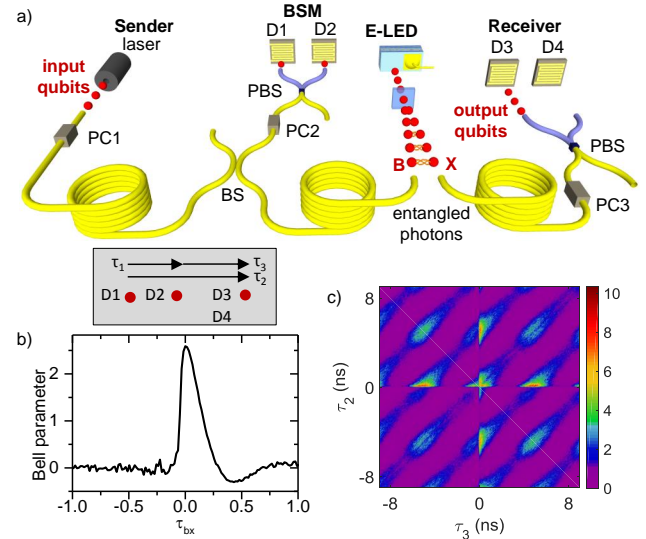


Figure 2: (a) Quantum relay experimental setup. The Sender encodes photons from an externally modulated laser diode with qubit states $|H\rangle, |V\rangle, |D\rangle, |A\rangle$, using a polarization controller PC1, to be transferred to the Receiver by quantum teleportation. Sender and Receiver are separated by ~ 1 km of fiber and a Bell-State Measurement (BSM) node in between. The BSM and Receiver share an entangled pair of photons emitted from the ELED. The input qubits interfere with biexciton photons on beamsplitter BS. Once detectors D1 and D2 measure their state, teleported output qubits are detected with a polarizing beamsplitter (PBS) at D3 and D4. All state calibrations at each node are done with polarization controllers (PC). (b) Bell parameter extracted from experimental data. (c) Average third-order correlation $g^{(3)}$. Pulsed character of the correlations is observed. The single-photon property of emission is seen as a dip in coincidences at $\tau_2 = \tau_3$. Higher three-photon coincidences running along $\tau_2 = 0$ and $\tau_3 = 0$ originate from elevated probability of the ELED emitting a pair of photons simultaneously.

lapses the formerly entangled *X* photon into a quantum state related to the input qubit together with a trivial unitary transformation[22]. In this work, input qubits of the form $\cos(a)|H_L\rangle + e^{ib}\sin(a)|V_L\rangle$ are teleported to the state $\cos(a)|V_X\rangle + e^{ib}\sin(a)|H_X\rangle$.

Theoretical analysis of the intricate time-dependent three-photon fields reveals a range of laser pulse conditions for which the calculated peak teleportation fidelities are close to optimum (Appendix). The laser pulse properties observed at detectors D1 and D2 were set accordingly, with integrated intensity of 0.85 relative to the *B* pulse, a fitted Gaussian FWHM of 0.95 ± 0.01 ns, and a delay of the laser pulse after the *B* pulse of 0.60 ± 0.02 ns relative to maximum overlap.

The entanglement properties of the photons emitted by the ELED were characterized within the quantum relay system. Second-order correlation measurements were performed in the rectilinear $\{H, V\}$ and diagonal $\{D, A\}$ linear polarization bases, where *D* and *A* represent the diagonal and anti-diagonal polarizations respec-

tively. From these measurements it is possible to determine Bell's parameter to indicate the degree of entanglement present[23, 24]. The result is shown in Fig. 2(b) as a function of the time delay τ_{BX} between a biexciton photon detected at D1 or D2, and an exciton photon at D3 or D4. For simultaneously detected photons, a Bell parameter of 2.59 ± 0.01 is observed, exceeding the limit of 2 for classical behavior, and corresponding to 91.8 % of the ideal value of $2\sqrt{2}$. To our knowledge, this is the first time entanglement has been distributed by a quantum dot source over a distance longer than a few meters.

The quantum relay was operated using polarization encoded BB84 quantum states[25], using the rectilinear and diagonal bases. Three-photon detection statistics were recorded between a pair of photons at D1 and D2, and one at D3 or D4. The polarizations of the input qubit and measurement basis, controlled by PC1 and PC3 respectively, were switched during the experiment so that a randomized sequence of teleported qubits could be recorded.

Fig. 2(c) shows the measured third-order correlation function $g^{(3)}$ averaged over all 4 polarization inputs, and over the corresponding co- and cross- polarized outputs. The horizontal and vertical axes are the time delays τ_2 and τ_3 between photon detection at D1 or D2 respectively, and a photon at D3 or D4. The intensity distribution has highly pulsed character, with peaks occurring when the delays τ_2 and τ_3 are an integer multiple of the ~ 4.9 ns repetition period. This is in contrast to previous reports of quantum teleportation with quantum dots, which operated in continuous mode. Stronger intensity peaks are observed for $\tau_2 = 0$ and $\tau_3 = 0$, as exciton emission directly following biexciton emission is enhanced. For coincident detection at D1 and D2, $\tau_2 = \tau_3$, a low intensity line indicates a suppression in detecting two B photons simultaneously due to the sub-Poissonian nature of the ELED source.

The polarization dependence of the quantum relay is evaluated from the difference between third-order correlation measurements with the expected, and unexpected (i.e. orthogonal to expected) output polarizations. Such $g^{(3)}$ contrast measurements are presented in Fig. 3 as a function of τ_2 and τ_3 for each of the input qubit states H,V,D, and A. High contrast at $\tau_2 = 0$ ($\tau_3 = 0$) is observed due to H (V) input laser photons exciting the D1 (D2) detector, so that contrast is dominated by correlation between X and a B photon at D2 (D1). The correlation contrast for D and A however looks quite different, dominated by a peak centered at $\tau_3 = \tau_2 = 0$, as two-photon interference between simultaneously detected photons is required for teleporting states in a superposition state. Calculations, shown in the right column, agree well with observations (Appendix).

The performance of the quantum relay is assessed by determining the relay fidelity F_P , which for each input photon state P is determined by:

$$F_P(\tau_3, \tau_2) = g_{P'}^{(3)}(\tau_3, \tau_2) / (g_{P'}^{(3)}(\tau_3, \tau_2) + g_{Q'}^{(3)}(\tau_3, \tau_2)),$$

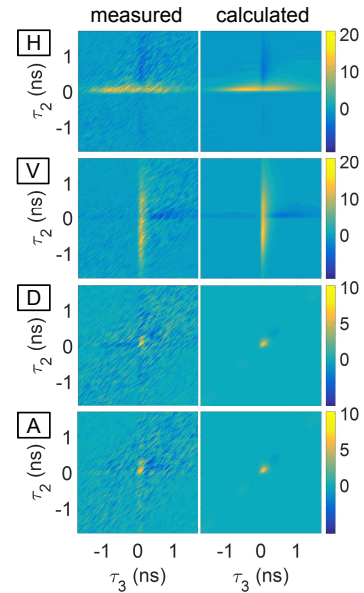


Figure 3: Difference between expected and unexpected third-order correlations $g^{(3)}$ as a function of photon detection time delays τ_2 and τ_3 . Measured and calculated results are shown in the left and right column respectively, corresponding to input states H, V, D, and A (from top to bottom).

where P' and Q' are the expected and orthogonal unexpected output polarizations respectively. Averaging across the four input states H,V,D, and A gives the average relay fidelity F , which is plotted in Fig. 4(a). A clear peak is observed around $\tau_2 = \tau_3 = 0$, where the fidelity clearly exceeds 0.75, the limit for optimal classical teleportation schemes using four-state protocols. Calculated behavior, shown in Fig. 4(b), shows similar features. The maximum measured value of F is more clearly observed in Fig. 4(c), which plots F as a function of τ_2 or τ_3 for simultaneous detection of two photons at the 'BSM' section. The peak rises to a maximum value of 0.900 ± 0.028 , exceeding the six-state average fidelity reported previously[18]. The corresponding measured individual relay fidelities are 0.957 ± 0.042 and 0.951 ± 0.0475 from polar states H and V, and 0.845 ± 0.064 , 0.847 ± 0.063 for superposition states D and A.

The high measured teleportation fidelities confirm that Sender and Receiver have shared information in excess of any information held by an eavesdropper. The difference between unity and the measured fidelity is the quantum bit error rate (QBER) of the shared key. Error correction protocols are known that can correct for QBER up to 0.2 in 4-state protocols[26], which corresponds to a minimum relay fidelity of 0.8, well below the experimentally measured value.

For smaller QBER, as in our experiment, more effective error correction protocols are available[27]. Using the single-photon, efficient BB84 protocol[28], in the limit of infinitely many signals shared by the users, the fraction R of secure bits that can be extracted from each detected

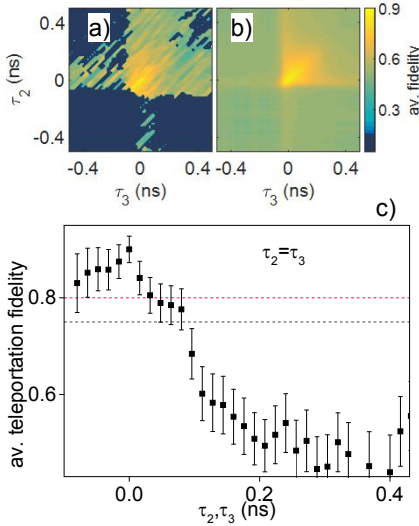


Figure 4: (a,b) Relay fidelity averaged across four input qubit states H, V, D, and A, as a function of the time delays τ_2 and τ_3 . (a) and (b) shown experimental and simulated results respectively. Note the measured fidelity is not defined some regions of the plot as no photons were detected due to the ELED or laser being ‘off’ (dark blue). (c) Average relay fidelity as a function of time delay τ_2 and τ_3 for $\tau_2 = \tau_3$. High fidelity points are concentrated around $\tau_2, \tau_3 = 0$, where the measured fidelity exceeds the classical limit of 0.75 shown by black dashed line. The threshold for 4-state error correction of 0.8 is shown as dashed red line.

photon is[29]:

$$R = 1 - h(Q_Z) - h(Q_X),$$

where h is the binary entropy function. By replacing the QBERs Q_Z and Q_X in the Z and X basis by those measured of 4.6% and 15.4% in the $\{H, V\}$ and $\{D, A\}$ bases respectively, we find that 0.111 secure key bits can be distilled from our Relay per detected photon.

A key advantage of quantum-dot based entangled light sources over spontaneous parametric down conversion

is that they can in principle operate ‘on-demand’ and deterministically deliver a single entangled photon pair when triggered, without detrimental additional pairs. In our experiments, we measure the second-order correlation for coincident X photons to be close to optimal at 0.046 ± 0.008 , highly suppressed from the Poissonian value of 1. Achieving maximal efficiency is predominantly limited by the photon collection efficiency, and the temporal post-selection window that heralds the occurrence of a teleportation event. Very high photon collection efficiencies have been reported in optically driven quantum dot nanostructures[30, 31], for which electrical injection schemes could be developed. Increasing the temporal region of high fidelity may be achieved by matching the laser and biexciton pulse shapes, reducing the fine-structure-splitting of 4.2 ± 0.1 μ eV, and extending the coherence time of the biexciton photons, which at 141.6 ± 4.2 ps limits the fidelity of teleporting D and A states.

In conclusion, we have reported the operation of a 203 MHz clocked quantum relay over 1 km of optical fiber using an electrically driven semiconductor light source. The measured relay fidelity of laser generated photonic qubits of 0.900 ± 0.027 exceeds both the threshold for quantum behavior, and the one for generating error corrected quantum keys with the BB84 protocol. Coupled with advances of quantum dot based entangled light sources at telecom wavelengths, our results suggest ELED technology could meet the need for a practical solution to create the backbone of future quantum networks.

Acknowledgments

The authors would like to thank M. Razavi for theoretical support and C. Panayi for useful discussions. The authors would like to acknowledge partial financial support through the UK EPSRC and the EU Marie Curie Initial Training Network Spin-optronics.

[1] N. Gisin, G. Ribordy, W. Tittel, and H. Zbinden, *Review of Modern Physics* **74**, 145 (2002).

[2] V. Scarani, H. Bechmann-Pasquinucci, N. J. Cerf, M. Dusek, N. Lutkenhaus, and M. Peev, *Rev. Mod. Phys.* **81**, 1301 (2009).

[3] D. Rosenberg, J. W. Harrington, P. R. Rice, P. A. Hiskett, C. G. Peterson, R. J. Hughes, A. E. Lita, S. W. Nam, and J. E. Nordholt, *Phys. Rev. Lett.* **98**, 010503 (2007).

[4] A. R. Dixon, Z. L. Yuan, J. F. Dynes, A. W. Sharpe, and A. J. Shields, *Appl. Phys. Lett.* **96**, 161102 (2010).

[5] S. Wang, W. Chen, J.-f. Guo, Z.-q. Yin, H.-w. Li, Z. Zhou, G.-c. Guo, and Z.-f. Han, *Optics Letters* **37**, 1008 (2012).

[6] B. Fröhlich, J. F. Dynes, M. Lucamarini, A. W. Sharpe, Z. Yuan, and A. J. Shields, *Nature* **501**, 69 (2013).

[7] M. Peev, C. Pacher, R. Alléaume, C. Barreiro, J. Bouda, Boxleitner, W. T. Debuisschert, E Diamanti, M. Dianati, J. F. Dynes, et al., *New Journal of Physics* **11**, 075001 (2009).

[8] A. K. Ekert, *Phys. Rev. Lett.* **67**, 661 (1991).

[9] S. L. Braunstein and S. Pirandola, *Phys. Rev. Lett.* **108**, 130502 (2012).

[10] H.-K. Lo, M. Curty, and B. Qi, *Phys. Rev. Lett.* **108**, 130503 (2012).

[11] Y.-L. Tang, H.-L. Yin, S.-J. Chen, Y. Liu, W.-J. Zhang, X. Jiang, L. Zhang, J. Wang, L.-X. You, J.-Y. Guan, et al., *Phys. Rev. Lett.* **113**, 190501 (2014).

[12] H.-J. Briegel, W. Dür, J. I. Cirac, and P. Zoller, *Phys. Rev. Lett.* **81**, 5932 (1998).

- [13] B. C. Jacobs, T. B. Pittman, and J. D. Franson, *Physical Review A* **66**, 052307 (2002).
- [14] H. de Riedmatten, I. Marcikic, W. Tittel, H. Zbinden, D. Collins, and N. Gisin, *Phys. Rev. Lett.* **92**, 047904 (2004).
- [15] X.-S. Ma, T. Herbst, T. Scheidl, D. Wang, S. Kropatschek, W. Naylor, B. Wittmann, A. Mech, J. Kofler, E. Anisimova, et al., *Nature* **489**, 269 (2012).
- [16] F. Bussières, C. Clausen, A. Tiranov, B. Korzh, V. B. Verma, S. W. Nam, F. Marsili, A. Ferrier, P. Goldner, H. Herrmann, et al., *Nature Photonics* **8**, 775 (2014).
- [17] G. Brassard, N. Lütkenhaus, T. Mor, and B. C. Sanders, *Phys. Rev. Lett.* **85**, 1330 (2000).
- [18] R. M. Stevenson, J. Nilsson, A. J. Bennett, I. Farrer, D. A. Ritchie, and A. J. Shields, *Nature Communications* **4**, 2859 (2013).
- [19] H.-K. Lo and H. F. Chau, *Science* **283**, 2050 (1999).
- [20] C. L. Salter, R. M. Stevenson, I. Farrer, C. A. Nicoll, D. A. Ritchie, and A. J. Shields, *Nature* **465**, 594 (2010).
- [21] J. Nilsson, R. M. Stevenson, K. H. A. Chan, J. Skiba-Szymanska, M. Lucamarini, M. B. Ward, A. J. Bennett, C. L. Salter, I. Farrer, D. A. Ritchie, et al., *Nature Photonics* **7**, 311 (2013).
- [22] C. H. Bennett, G. Brassard, C. Crépeau, R. Jozsa, A. Peres, and W. K. Wootters, *Phys. Rev. Lett.* **70**, 1895 (1993).
- [23] J. F. Clauser, M. A. Horne, A. Shimony, and R. A. Holt, *Phys. Rev. Lett.* **23**, 880 (1969).
- [24] R. J. Young, R. M. Stevenson, A. J. Hudson, C. A. Nicoll, D. A. Ritchie, and A. J. Shields, *Phys. Rev. Lett.* **102**, 30406 (2009).
- [25] C. H. Bennett and G. Brassard, *Proceedings of the IEEE International Conference on Computers, Systems and Signal Processing*, Bangalore, India, IEEE, New York pp. 175–179 (1984).
- [26] H. F. Chau, *Phys. Rev. A* **66**, 060302(R) (2002).
- [27] G. Brassard and L. Salvail, in *Advances in Cryptology - EUROCRYPT '93, Lecture Notes in Computer Science* 765, edited by T. Helleseth (Springer-Verlag Berlin Heidelberg, 1994), pp. 410–423.
- [28] H.-K. Lo, H. F. Chau, and M. Ardehali, *J. Cryptology* **18**, 133 (2005).
- [29] M. Koashi, *New Journal of Physics* **11**, 045018 (2009).
- [30] A. Dousse, J. Suffczynski, A. Beveratos, O. Krebs, A. Lemaître, I. Sagnes, J. Bloch, P. Voisin, and P. Senellart, *Nature* **466**, 217 (2010).
- [31] J. Claudon, J. Bleuse, N. S. Malik, M. Bazin, N. Gregersen, C. Sauvan, P. Lalanne, and J.-M. Gérard, *Nature Photonics* **4**, 174 (2010).
- [32] T. Legero, T. Wilk, A. Kuhn, and G. Rempe, *Applied Physics B* **77**, 797 (2003).
- [33] C. Santori, D. Fattal, J. Vuckovic, G. S. Solomon, and Y. Yamamoto, *New Journal of Physics* **6**, 89 (2004).

Appendix

Entangled light source

Entangled-photon pairs are generated by an InAs quantum dot, embedded in a 2-lambda GaAs optical cavity within a p-i-n heterostructure grown by MBE. In

order to improve light collection, 6 top and 18 Bragg reflectors (DBRs) were grown. The relatively small dimensions of the mesa (210x110 μm) allow for a simple direct bonding design, while increasing the pulsed operation performance compared to previously reported, larger, entangled-LEDs. The dot density is low enough so that no apertures were required and the light was collected using a single-mode fiber. The ELED device was driven by electrical injection at a frequency of 203 MHz, in forward-bias, with a modulating a.c. voltage of nominally square pulses with 0.4 V amplitude and 490 ps width, at a temperature of 19.7 K. The emission spectrum of the dot under these conditions shows the biexciton B and exciton X at 885.7 and 887.3 nm respectively. The fine-structure-splitting was $4.2 \pm 0.1 \mu\text{eV}$.

Quantum relay

For the input qubit photons at the Sender section, a CW laser was externally modulated and synchronized with the dot driving frequency using a Mach-Zehnder optical intensity modulator. The generated pulses can have a FWHM of $0.60 \pm 0.02 \text{ ns}$. The relative time-integrated intensities between laser and biexciton photons incident on detectors D1 and D2 was set to 0.85:1. The input qubit polarization state was selected using a pseudo-random number generator and polarization controller PC1 at a frequency exceeding the 3-photon coincidence rate. We note that the system is in principle compatible with quantum random number generators and phase modulation at frequencies exceeding the input qubit rate. The logical teleportation states $\{H, V\}$ are calibrated to the quantum dot's polarization eigenbasis, and the diagonal states $\{D, A\}$ are set at $+/ - 45^\circ$ to the rectilinear basis using a linear polarizer.

A 95:5 fiber beamsplitter was used to interfere the input laser photons with the biexciton photons. We only look at events from one output arm of this beamsplitter which maximizes the fraction of ELED photons detected in our experiment. The system was actively stabilized using electrical polarization controllers at each of the sections during the experiment. The degree of polarization for the input control qubits was maintained at $97.5 \pm 1.5\%$. The 5% output port was used to spectrally tune the laser to the biexciton wavelength using a grating spectrometer, with an average detuning of $0.12 \pm 1.68 \mu\text{eV}$ throughout the experiment.

Finally, photons at the BSM and Receiver polarizing beamsplitters (PBSs) were detected using four superconducting detectors (SSPDs). The timing jitter between pairs of detectors was approximately Gaussian with FWHM of $58.4 \pm 2.5 \text{ ps}$, with single photon counting hardware resolution of 16ps.

Three-photon correlations

Three-photon coincidences were recorded corresponding to 2 photons at BSM detectors D1 and D2, with polarization H and V, with one photon at either Receiver's detectors D3 and D4. D3 and D4 record both expected photons with polarization P' and unexpected output photons with polarization Q' simultaneously.

The detection times at each detector are defined as t_1 (D1), t_2 (D2), and t_3 (D3 & D4). All events were recorded relative to detections at D1 (H polarized photons). Third-order correlations $g^{(3)}$ for each output polarization were determined from the normalized statistics of the three photon coincidences, as a function of two time delays, $\tau_2 = t_3 - t_1$ and $\tau_3 = t_3 - t_2$. We note that the choice of which pair of time delays amongst 3 photons to choose is somewhat arbitrary, for example $t_2 - t_1$ and $t_3 - t_1$ have been used in previous reports.

Error analysis

Errors are dominated by Poissonian counting statistics, which determines the errors on the third-order correlations from the number of photons detected. Errors are propagated to determine the relay fidelity errors of individual input states, and the average relay fidelity. Systematic errors due to the temporal calibration and resolution of our system are also included in the fidelity measurements, but are almost negligible. Note that all experimental 3-photon results are presented for a time-integration window of 32×112 ps in τ_1 and τ_2 respectively, and evaluated on a 16 ps grid, so adjacent points are not independent.

Calculation of time-dependent $g^{(3)}$ correlations

In our experiments, we employ a beamsplitter to combine laser photons with biexciton photons originating from an entangled-LED, as shown in figure 5(a). To conserve biexciton photons from the entangled light source, the beamsplitter is highly imbalanced such that the transmission coefficient $|k_t| \gg |k_r|$. Only photons emerging on the efficient arm of the beamsplitter are measured, so for simplicity, the transmission and reflection coefficients of the beamsplitter, and phase change due to the coupling, are included within the amplitude and overall phase components of the laser and quantum dot wavefunction ψ_L and ψ_{BX} .

To begin, we define the laser and quantum dot states. In general, they are given by:

$$\psi_j = A_j(t_j)C_j(t_j)|\Psi_j(t_j)\rangle,$$

where $A_j(t_j)$ is the time dependent real amplitude, $C_j(t_j)$ is the overall phase, and $|\Psi_j(t_j)\rangle$ the polarisation and any polarisation dependent phase. The overall phase term is further defined as:

$$C_j(t_j) = e^{i\omega_j t_j} e^{i\phi_j(t_j)}.$$

The first exponent is coherent, and contributes to the final solutions only through detuning of ω_j to the primary frequencies ω_B and ω_X . Decoherence is represented by random fluctuations of the phase ϕ_j as a function of time t_j , such that $\langle e^{i[\phi_j(t_j) - \phi_j(t_j + \Delta)]} \rangle = e^{-|\Delta|/T_j}$, where T_j is the coherence time of photon j [32, 33].

For the laser input state with polarization defined by real parameters a and b , we have:

$$\begin{aligned} \psi_L &= A_L(t_L)C_L(t_L)|\Psi_L\rangle, \\ |\Psi_L\rangle &= \cos(a)|H\rangle + e^{ib}\sin(a)|V\rangle. \end{aligned}$$

The output polarization state is:

$$|\Psi_Q\rangle = \cos(x)|H\rangle + e^{iy}\sin(x)|V\rangle.$$

For photon pairs from the quantum dot, we have:

$$\psi_{BX} = A_{BX}(t_B, t_X)C_B(t_B)C_X(t_X)|\Psi_{BX}(t_B, t_X)\rangle.$$

The ideal quantum dot biphoton amplitude and state are given by

$$\begin{aligned} A_{BXe}(t_B, t_X), \\ |\Psi_{BXe}\rangle = (e^{is(t_X - t_B)}|HH\rangle + e^{-is(t_X - t_B)}|VV\rangle)/\sqrt{2}. \end{aligned}$$

In practice, however, the emission from the quantum dot is partially mixed. We approximate this with the amplitude $A_{BXu}(t_B, t_X)$ and equal mixture of the polarization states:

$$\begin{aligned} \Psi_{HH} &= e^{is(t_X - t_B)}|HH\rangle, \\ \Psi_{HV} &= e^{is(-t_X - t_B)}|HV\rangle, \\ \Psi_{VH} &= e^{is(t_X + t_B)}|VH\rangle, \\ \Psi_{VV} &= e^{is(-t_X + t_B)}|VV\rangle. \end{aligned}$$

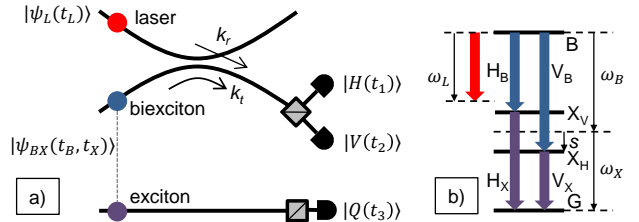


Figure 5: (a) Schematic of quantum relay scheme. Laser and biexciton photons meet at a fiber optic coupler with transmission and coupling amplitudes k_t and k_r , before direction by a polarizing beamsplitter to a pair of photon detectors. The exciton photon polarization is selected in a given state Q , and measured by a third detector. (b) Level diagram showing the biexciton (B), exciton (X) and ground (G) states of a single quantum dot, plus the input laser photon. Frequencies and detunings of various photon states are shown.

The joint amplitude of the electric field at the three photon detectors Z is given by the following equation, where four-photon contributions and higher are disregarded due to their relatively small probability compared to three-photon events:

$$\begin{aligned} Z(t_1, t_2, t_3) = & \langle H | \psi_L(t_1) \langle VQ | \psi_{BX}(t_2, t_3) \rangle \\ & + \langle V | \psi_L(t_2) \rangle \langle HQ | \psi_{BX}(t_1, t_3) \rangle \\ & + \langle HV | \psi_{LL}(t_1, t_2) \rangle \langle Q | \psi_X(t_3) \rangle \\ & + \langle HVQ | \psi_{BBX}(t_1, t_2, t_3) \rangle. \end{aligned}$$

The first two terms are the desired three-photon amplitudes originating from a single laser, biexciton, and exciton photon. The third and fourth terms originate from two laser photons plus one exciton photon, and two biexciton photons plus one exciton photon respectively.

The three-photon intensity $Z(t_1, t_2, t_3)Z^*(t_1, t_2, t_3)$ is evaluated and integrated over the arrival time of the X photon t_3 , from which we drop the subscript for convenience. Finally, we make substitutions of the form:

$$\begin{aligned} \eta_j I_j(t_j) &= A_j^2(t_j), \\ \eta_j \eta_k g_{jk}^{(2)}(t_j, t_k) &= A_{jk}^2(t_j, t_k), \\ \eta_j \eta_k \eta_l g_{jkl}^{(3)}(t_j, t_k, t_l) &= A_{jkl}^2(t_j, t_k, t_l), \end{aligned}$$

where η_j is the time averaged intensity of photon j , and $I_j(t_j)$ the normalised intensity of photon j as a function of time. The final expression for the third-order correlation is,

$$\begin{aligned} g^{(3)}(\tau_2, \tau_3) \propto & \frac{1}{2} \cos^2(a) \sin^2(x) \int_0^p I_L(t - \tau_2) g_{BXe}^{(2)}(t - \tau_3, t) dt \\ & + \frac{1}{2} \sin^2(a) \cos^2(x) \int_0^p I_L(t - \tau_3) g_{BXe}^{(2)}(t - \tau_2, t) dt \\ & + \frac{1}{4} \sin(2a) \sin(2x) e^{-\frac{|\tau_1|}{T_L} - \frac{|\tau_1|}{T_B}} \\ & \times \cos((\omega_B - \omega_L)\tau_1 - s(\tau_3 + \tau_2) + y + b) \\ & \times \int_0^p \sqrt{(I_L(t - \tau_2) I_L(t - \tau_3) g_{BXe}^{(2)}(t - \tau_2, t) g_{BXe}^{(2)}(t - \tau_3, t))} dt \\ & + \frac{1}{4} \cos^2(a) \int_0^p I_L(t - \tau_2) g_{BXu}^{(2)}(t - \tau_3, t) dt \\ & + \frac{1}{4} \sin^2(a) \int_0^p I_L(t - \tau_3) g_{BXu}^{(2)}(t - \tau_2, t) dt \\ & + \frac{\eta_L}{\eta_B} \frac{1}{4} \cos^2(a) \sin^2(a) \int_0^p g_{LL}^{(2)}(t - \tau_2, t - \tau_3) I_X(t) dt \\ & + \frac{\eta_B}{\eta_L} \int_0^p g_{BBX}^{(3)}(t - \tau_2, t - \tau_3, t) dt. \end{aligned}$$

Note the final term containing $g_{BBX}^{(3)}(t - \tau_2, t - \tau_3, t)$ is evaluated by substitution with chains of two-photon correlations, for different ordering of the two biexciton and one exciton photons. This is justified as detection of the first photon places the system to a well-defined state, which serves as the starting point for a correlation to a second photon, which after detection again places the system into another well-defined state, which is the starting point with correlation to a third photon. A factor of $1/2$ in the penultimate term accounts for the Poissonian statistics of the laser two-photon intensity.

Optimum teleportation conditions

The single laser photon envelope I_L was approximated as a Gaussian function, which is a satisfactory approximation of what we observe in experiment. Single biexciton and exciton photon intensities $I_B(t_B)$ and $I_X(t_X)$ were directly measured, and the fine-structure-splitting and biexciton coherence time determined from polarization dependent spectroscopy and single-photon interferograms respectively. Correlations were measured between biexciton and exciton photons to determine $g_{BX}^{(3)}(t_B, t_X - t_B)$ for co- and cross-linearly polarized states. The entangled and unentangled biphoton fractions $g_{BXe}^{(2)}$ and $g_{BXu}^{(2)}$ were extracted from half the difference between, and uncorrelated component of, these measurements respectively. Similarly correlations between pairs of biexciton photons $g_{BB}^{(2)}(t_1, t_2)$ were directly measured.

Note that imperfections in polarization recovery and timing jitter are well represented in the parameter data, as the same physical measurement system was used for their measurement as for teleportation. However, additional jitter was added when evaluating the calculations to terms with discontinuities around zero delay. This fact, together with the lower time-averaged estimate of the coherence time compared to biexciton photons emitted in a single cycle, means that calculations are expected to underestimate the relay fidelity slightly, as observed.

In order to maximize the relay fidelity in experiments, the expected maximal fidelity was calculated as a function of laser pulse intensity, width, and delay relative to the biexciton photon. The results are summarized in figure 6, which plots the calculated relay fidelity as a function of the pulse delay and width (a), with corresponding optimal laser intensity in (b). Highest fidelities are observed for a laser delayed between -0.6 and 0.8 ns relative to maximal overlap with the biexciton state, and for a pulse width between 0.45 and 2.05 ns. The values employed in our experiments are within this range.

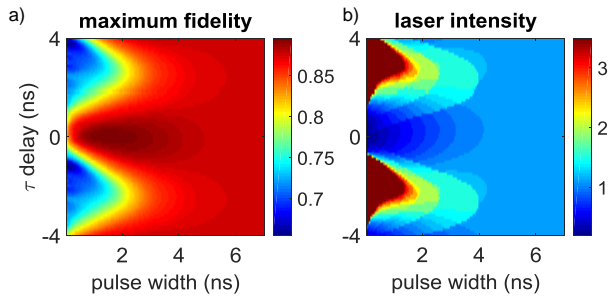


Figure 6: (a) Calculated maximum relay fidelity for our ELED with Gaussian laser pulses as a function of laser pulse width and delay relative to the biexciton photon. (b) Corresponding laser relative to biexciton intensity required (up to a limit of 3.5) to achieve maximal fidelity.